Comprehensive Static Characterization of Vertical Electrostatically Actuated Polysilicon Beams

E. K. Chan, K. Garikipati, and R. W. Dutton

CISX 305, Center for Integrated Systems

Stanford University

Stanford, CA 94305-4075

Email: edward_chan@alumni.stanford.org

Tel: (650) 723-1482 Fax: (650) 725-7731

Abstract

The entire process of calibrating an electromechanical simulator – identifying relevant parameters, designing and measuring test structures, extracting parameters using detailed electromechanical simulations, and extrapolating the behavior of an actual device – is presented. The simulation model for electrostatically actuated beams is calibrated to a wide range of electrical and optical measurements of test structures, and is then used to predict the behavior of more complex dual-bias-electrode structures. Various mechanical discontinuities, and post-buckled pull-in behavior are addressed explicitly. Arbitrary fitting coefficients that limit generality are avoided. The well-characterized behavior of the dual-electrode structures can serve as verification test cases for evaluating coupled electromechanical simulators.

Index terms

electromechanical, polysilicon, material properties, buckling, gold

1. Introduction

Electrostatically actuated beams are widely used and studied in the microelectromechanical systems (MEMS) community. Such beams are used as relays, oscillators, filters, grating light valves, tunable capacitors and probe arms [1]. Computer simulation tools such as Abaqus [2], IntelliCAD and MEMCAD are being used increasingly to design and understand the behavior of these complex devices. These tools need to be thoroughly calibrated to particular fabrication processes in order to produce

useful and accurate results. Researchers have been measuring resonant frequencies [3], observing the effects of stress on rotating or buckling structures [4], probing beams with mechanical profilers [5], measuring displacements under electrostatic forces [6], and performing traditional uniaxial tensile tests [7] to determine material properties. The reported properties vary considerably for a given material, even for the polysilicon layer in the widely-used Multi-User MEMS Procesess (MUMPs) [8]. These variations could be due to errors and approximations in measurements and modeling, or due to actual variations in material properties depending on actuation method, actuation direction, specimen size and sample preparation. Ideally, running a whole battery of parameter extraction methods on test structures on a single die would reveal a unique and universal set of material parameters. Each method has limited resolution, however, making it difficult to make definitive comparisons, or to quantify phenomena such as anisotropy.

This paper unifies two different parameter extraction methods to generate a consistent simulation model calibrated to the MUMPs process. The simulation model is calibrated to optical (buckling amplitude) and electrical (pull-in voltage) measurements concurrently, not independently as in [4] and [6], thus increasing confidence in the extracted parameters. A simulation-based model consisting of geometrical and material property information precludes the need for rather ad hoc parametric adjustments and simplifying assumptions. The calibration steps shown in Fig. 1 consist of identifying relevant simulation model parameters, designing suitable test structures, measuring geometry then extracting parameters using detailed yet fast electromechanical simulations, and finally extrapolating the behavior of an actual complex device. This paper targets electrostatically actuated beams fabricated in the POLY1 layer although the model parameters can be used to simulate other devices. However, one must be cautious whenever simulating different modes of actuation or regimes of operation, or devices with dimensions beyond the range of the calibration. Material properties cannot always be extrapolated.

In the text that follows, the MUMPs system of materials and the 2-D simulation model in Abaqus are introduced. Every calibration procedure is necessarily limited to a range of devices and dimensions. This paper examines in detail vertical electrostatically actuated 30-μm-wide polysilicon fixed-fixed beams with stepups and other discontinuities. Geometrical dimensions are first measured then initial biaxial stress and Young's modulus are extracted from pull-in voltages and buckling amplitudes. The observed transition in pull-in behavior of post-buckled beams beyond a threshold beam length is detailed. The calibration steps are then repeated for beams with steps over underlying POLY0 pads, and beams with dimples. The well-characterized simulation model is then extended to predict the behavior of dual-bias-electrode structures. The extrapolation is very good, verifying the accuracy of the calibration methodology.

2. Materials System

2.1 Fabrication overview

Fig. 2 shows the cross section of an electrostatically actuated beam fabricated in MUMPs. In this surface micromachining process, a 0.6-μm film of silicon nitride, serving as a dielectric isolation layer, is deposited first on a heavily-doped silicon substrate. The first layer of polysilicon, a 0.5-μm-thick layer of POLY0, is then deposited on the nitride and patterned using Reactive Ion Etching (RIE). This patterning step also thins down exposed areas of silicon nitride. 2 μm of sacrificial phosphosilicate glass (PSG) is put down next. Portions of the PSG are then etched through so that polysilicon deposited later can be anchored to the nitride or POLY0 layers. This anchor etch overetches about 0.13 μm of nitride and about 0.02 μm of POLY0. A shorter, well-controlled PSG etch of about 0.75 μm creates dimples. The main structural layer, 2 μm of polysilicon (POLY1), is then deposited and patterned. In addition to the stepup anchors, the conformal polysilicon layer can have steps over POLY0 pads, and steps down into dimples which affect beam behavior. Another layer of PSG and another layer of polysilicon are deposited and patterned after this but are not shown in Fig. 2. Gold is the final layer, deposited for probing and electrical routing. At the end, the sacrificial PSG is etched away in an HF solution releasing the POLY1 layer leaving freestanding beams anchored to the nitride or POLY0. An electrochemical potential set up during this wet release step results in uneven overetching of the polysilicon layers causing effects described later in this paper.

Measurements in this paper were made on a single die on the MUMPs 29 run unless noted otherwise. The die was supercritically dried after a 1.5 minute HF release to

obtain long freestanding beams. Rather than trying to extract parameters in light of run-to-run or even die-to-die variations, the goal of this paper is to come up with very accurate geometric and material properties, and hence to validate two consistent parameter extraction methodologies and their underlying coupled electromechanical simulation model.

2.2 Thicknesses and Geometry

The geometric properties of interest are the thicknesses of the POLY0, POLY1, nitride and sacrificial PSG layers, the depth of the dimple, and the shape of the stepup anchors and other steps. Accurate measurements of true final thicknesses are challenging because of overetching, and can be significantly different from measurements of blanket films deposited on a silicon wafer.

The electrical thickness of the nitride is determined from the capacitance between a POLY0 pad and the substrate. This thickness is an upper bound since the nitride that is not under POLY0 is thinned down during the POLY0 and PSG etches. Using a Zygo NewView 200 surface profiler, the thickness of the POLY1 layer is measured at the base of a stepup anchor deposited on POLY0 as shown in the Scanning Electron Micrograph (SEM) of Fig. 3. The overetch of about 0.02 μm of the underlying POLY0 pad during the anchor etch causes the measured thickness to be slightly less than the true thickness of a freestanding POLY1 beam. This discrepancy is offset in part by the overetch of the underside of a beam during the HF release, and by surface roughness which adds to optical thickness measurements but not to structural rigidity. An alternate measurement is the height of a released POLY1 beam pegged to a POLY0 layer. This measurement, however, includes the effects of surface residue which can be significant. All dimensions used in subsequent simulations are shown in Table 1. The thickness of the POLY0 layer is measured with respect to the exposed nitride surface thus including the nitride overetch as shown in Fig. 2. The sacrificial gap is determined by subtracting the thickness of the POLY1 layer from the height of an unreleased POLY1-plus-PSG stack deposited on POLY0.

Interferometric measurements show that POLY0 layers connected to gold pads are about 0.01 μm thinner, and have rougher surfaces and hence lower reflectivity than unconnected POLY0 layers. This is due to an electrochemical potential set up by the gold pads that increases the etch rate of the POLY0 layer during the HF release etch. The influence of a gold pad depends on the amount of exposed surface area of the polysilicon part that it is connected to. This slight etching of the POLY0 layer causes the sacrificial gap between the POLY0 and POLY1 to be about 0.01 μm larger than the gap between the nitride and POLY1. It is difficult to accurately determine how much the thicknesses of the POLY1 layers are affected although other effects of gold are visible in Figs. 4 and 5. Three similarly-designed POLY1 cantilevers are shown in Fig. 4 with the only difference being that the center cantilever is connected to a gold pad. That center cantilever curls up more than the other two cantilevers. In Fig. 5, the center fixed-fixed beam that is connected to gold buckles 0.6 μm higher than the other 700 μm beams that are not connected to gold indicating an increase of 1.5 MPa in the initial biaxial stress of the beam. The top surface of the center beam, which is surmised to be at a low stress level, was etched away more quickly in the HF than the surfaces of the other beams leaving behind a beam with higher average stress. Thus, the presence of gold induces non-uniformity among ostensibly similar devices. To prevent such area-dependent effects, all polysilicon parts measured in this paper are not connected to gold pads unless noted otherwise.

2.3 Dependence on beam width

The behavior of the beams also shows a dependence on their widths. Fig. 6 is an interferometric image of an array of cantilevers of similar length but of varying widths. The beams, all without connections to gold, curl down with different radii of curvature with the exception of the anomalous 10-μm-wide beam which actually curls up. The narrower the beams, the more susceptible the behavior of the beams are to small deviations in the cross section from an ideal rectangular shape. In addition, each of the beams exhibits variations in height along its width as shown in the cross-sectional profile. The top surfaces of the narrower beams (30-μm-wide or less) are rounded. This roundedness is probably due to uneven etching of the surface during the patterning step rather than due to bending. Bending in such a deformation mode – widthwise curling without significant curling along the length – cannot be simulated using isotropic stress gradients. The wider beams show saddle-like height variations along their widths with rounded ridges near each edge. It is possible that the two ridges coalesced into one

mound in the case of the narrower beams. Variations in degree of curvature were observed from die to die but the general trends shown in Fig. 6 are universal. Since the source of such widthwise variations is unclear, only 30-μm-wide beams are used for the calibration to minimize the effects of non-ideal cross sections while avoiding saddle-like height variations. The performance of fixed-fixed beams studied here are only marginally affected by variations in height and curvature of the observed magnitudes. The characterization of cantilever beams is more involved, however, and requires more investigation.

3. Calibration

3.1 Simulation model

Fig. 7 shows the profiles of electrostatically actuated beams – flat beams, beams over POLY0, and dimpled beams. For the best match to simulations, the beams were designed to be essentially extruded two-dimensional profiles [9]. The 2-D simulation model in Abaqus is shown in Fig. 8 highlighting the geometry of the stepup anchors and other mechanical discontinuities which correspond to the SEMs of Figs. 3 and 9. The effects of overetch, sloping sidewalls and conformal deposition are included. Abaqus is a finite element package which solves the equations of solid mechanics describing the bending and stress of the beam under various loading conditions. Electrostatic forces, using parallel-plate approximations that account for the effects of fringing fields and finite beam thickness, are incorporated as user-defined loads allowing Abaqus to solve fully-coupled electromechanical problems [2], [9]. Full three-dimensional (3D) simulations consume enormous computing resources and time, making them infeasible for parameter extraction procedures which require the solutions of many variations of a given system.

3.2 Buckling amplitude

The POLY1 layer in MUMPs is deposited slightly compressive. As a result, beams fabricated in POLY1 tend to deform to relieve some of that stress. Buckling amplitude depends on beam length, beam thickness and boundary conditions. In contrast to the case with perfectly clamped boundaries where deflection occurs only beyond a threshold buckling beam length, beams with stepup anchors deform even at shorter lengths. This is shown in Fig. 10 where buckling amplitudes of flat beams along with their corresponding pull-in voltages are plotted as functions of beam length. The transition from the pre-buckled state to the post-buckled state is not abrupt. Since the buckling amplitude depends strongly on initial strain but not at all on Young's modulus, the strain parameter can be extracted by fitting Abaqus simulations to the measured buckling amplitudes for various beams. The measurements were made with the Zygo interferometer using POLY0 layers instead of the nitride as reference levels to minimize the effects of secondary fringes and poor reflectivity. The excellent fit indicates that the other two parameters critical to buckling amplitude – boundary conditions and beam thickness – were accurately determined from interferometric measurements and SEMs.

3.3 Pull-in voltage

When a voltage is applied between the beam and silicon substrate as shown in Fig. 7(a), an electrostatic force pulls the beam towards the substrate. Beyond a threshold voltage called the pull-in voltage, the beam snaps down abruptly and contacts the nitride dielectric. Both Young's modulus and residual stress can be extracted by fitting simulation results to pull-in voltage measurements. An HP 4275A capacitance-voltage (CV) meter was used to apply a bias voltage and to sense the abrupt increase in capacitance at pull-in. The stress parameter extracted from these measurements is consistent with that determined in the previous section. The extracted Young's modulus for these beams is 138 GPa which is consistent with what was obtained for a previous MUMPs run [9], and also similar to what was obtained by Sharpe et al. [7] but somewhat lower than that obtained by Gupta [6].

The simulation fit is good with the kink at 620 μm captured accurately as shown in Fig. 10. The three types of pull-in behavior corresponding to the regions in Fig. 10 are shown in Fig. 11. Pressure due to micropositioned probes affect buckling amplitudes and should be minimized. A short beam in Region I will deflect continuously with increasing voltage until the gap decreases to about 1.0 μm then snap down to the nitride dielectric. A longer beam in Region II that has an initial buckling displacement deflects continuously then snaps down to a stable state below the zero-displacement position. From there, it continues to deflect with increasing voltage before finally snapping down again, this time contacting the nitride. This two-step phenomenon does not occur for longer beams in

Region III because there is no stable state below zero-displacement so the beams snap down all the way to the nitride. In contrast to beams in the first two regions, beams exhibiting this third type of behavior have pull-in voltages that increase with beam length because the buckling amplitudes and hence the effective gaps increase with beam length. With the additional dependence of effective gap on initial stress, the pull-in voltages of these post-buckled beams are more sensitive to initial stress than the pull-in voltages of shorter beams.

3.4. Calibration of beams with multiple discontinuities

Beams fabricated out of conformal polysilicon can have steps over underlying POLY0 layers, and dimples as shown in Fig. 7(b) and (c) thus requiring two additional model parameters – dimple depth and POLY0 thickness. These parameters were measured interferometrically then included in the Abaqus model using the SEM of Fig. 9 as a guide to the actual shape of the discontinuities. The beams over POLY0 behave quite similarly to flat beams. The total effective gap is smaller due to the absence of the nitride dielectric resulting in slightly lower pull-in voltages. The transition in buckling amplitudes from the pre-buckled to the post-buckled states is more gradual and begins earlier due to the increased compliance near the boundaries. The amplitudes are also slightly smaller. The same three regions of pull-in behavior are observed. On the other hand, the characteristics of beams with dimples deviate rather significantly from those of flat beams. The dimples cause the beams to buckle downwards systematically instead of upwards. Therefore, the post-buckled pull-in voltages do not rise with beam length but instead go to zero once the beams buckle into contact with the nitride. As for the beams over POLY0, the transition from pre-buckled to post-buckled states is more gradual and occurs earlier. The pull-in voltages are lower compared to flat beams of similar length because the effective gap is smaller by the dimple depth.

4. Extrapolation to dual-bias-electrode structures

The simulation model characterized in the previous sections is then used to predict the behavior of more complex dual-bias-electrode structures shown by the 3-D solid model of Fig. 12. This design can be the basis of a tunable capacitor or oscillator. The measurements of Fig. 13 are of pull-in voltages (V_{pi}) at one electrode as a function of bias voltages (V_{bias}) applied to the other electrode for three different devices. Pull-ins were sensed using a CV meter. The bias electrodes were designed close enough to the center of the beam such that pull-in is still abrupt despite the fact that the beam is being leveraged downwards by the electrodes. These devices incorporate all the types of discontinuities characterized earlier. By having two bias electrodes, multiple precise pull-in voltage measurements can be used to characterize a single device. The dimple at the center of the beam prevents conductor-to-conductor contact. Dielectric charging should not affect the measurements since there is no applied electric field across exposed regions of nitride thus allowing quick consecutive measurements [9]. The V_{pi} vs V_{bias} curves for the devices with left and right electrodes of equal length are symmetric about the $V_{pi} = V_{bias}$ line. By swapping the bias and pull-in connections, the integrity of the devices can be verified by checking for symmetry.

The extrapolated behavior matches the measurements very well. For curves such as these with segments that are primarily vertical, error norms should be calculated along the directions normal to the curves as shown in Fig. 13 rather than simply taking the differences between the measured and simulated pull-in voltages at a particular bias voltage. Using this normal-direction error metric, the simulations match the measured values to within 2%. We have thus demonstrated that these comprehensive calibration procedures using simple test structures produce simulation model parameters that predict the behavior of more complex devices very accurately. Therefore, the model parameters in Table 1 along with the measurement data in Fig. 13 can serve as verification test cases to evaluate the accuracy of coupled electromechanical simulators.

5. Conclusions

A comprehensive methodology to calibrate a simulation model to the MUMPs process has been presented. Interferometric measurements, SEMs and electrical measurements of simple test structures along with detailed electromechanical simulations were used to determine material and geometrical parameters especially pertinent to vertical electrostatically actuated beams. The limits of the calibration procedure due to width-dependent variations and the effects of gold pads were discussed. The extrapolations of the simulation model to more complex devices were excellent demonstrating the viability of the dual-bias-electrode structures to serve as canonical

benchmarks for coupled electromechanical simulators. Further work is necessary to uncover and characterize unanticipated non-uniformities among ostensibly similar structures, especially for cantilevers that are much more sensitive to stress gradient variations than fixed-fixed beams.

Acknowledgements

The authors would like to thank B. K. Eplett for help with the SEMs. This work was supported by the DARPA Composite CAD program (contract #F30602-96-2-0308-P00001).

References

[1] Proceedings of the IEEE, Special Issue: Integrated Sensors, Microactuators, and Microsystems (MEMS), Aug. 1998.

[2] Hibbitt, Karlsson and Sorensen, Inc., ABAQUS/Standard User's Manual, version 5.6, Pawtucket, 1996.

[3] K. E. Petersen, "Dynamic micromechanics on silicon: Techniques and devices," *IEEE Trans. Electron Devices*, ED-25, pp. 1241-1250, 1978.

[4] W. Fang, J. A. Wickert, "Post-buckling of micromachined beams," *Journal of Micromechanics and Microengineering*, vol. 4 no. 3, pp. 116-122, Sep. 1994.

[5] T. P. Weihs, S. Hong, J. C. Bravman, W. D. Nix, "Mechanical deflection of cantilever microbeams: A new technique for testing the mechanical properties of thin films," *Journal of Materials Research*, 3 (5), pp. 931-942, Sep./Oct. 1988.

[6] R. K. Gupta, "Electrostatic pull-in test structure design for in-situ mechanical property measurements of microelectromechanical systems (MEMS)," Ph.D. thesis, Massachusetts Institute of Technology, USA, June 1997.

[7] W. N. Sharpe, Jr., K. Turner, R. L. Edwards, "Measurements of the effect of specimen size on Young's modulus and tensile strength of polysilicon," in *Late News Poster Session Supplemental Digest of IEEE Solid State Sensor and Actuator Workshop*, Hilton Head, pp. 17-19, June 1998.

[8] D. A. Koester, R. Mahadevan, A. Shishkoff, K. W. Markus, SmartMUMPs Design Handbook including MUMPs Introduction and Design Rules (rev. 4), Microelectronics Center of North Carolina, July 1996.

[9] E. K. Chan, K. Garikipati, R.W. Dutton, "Characterization of contact electromechanics through capacitance-voltage measurements and simulations," *Journal of Microelectromechanical Systems*, vol. 8 no. 2, pp. 208-217, June 1999.

[10] N. M. Wilson, R. W. Dutton, P. M. Pinsky, "Utilizing existing TCAD simulation tools to create solid models for the simulation-based design of MEMS devices," *Proceedings of ASME International Mechanical Engineering Congress and Exposition*, Anaheim, DSC-vol. 66, pp. 565-570, Nov. 1998.

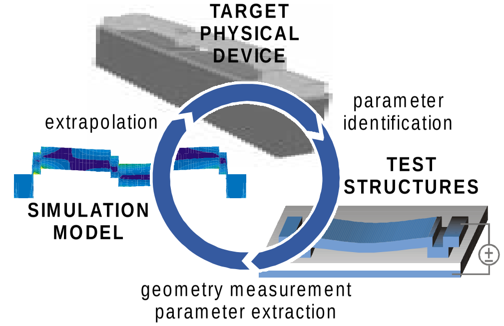

Figure 1. Simulator calibration steps for accurate simulation results. The goal is to help optimize device designs.

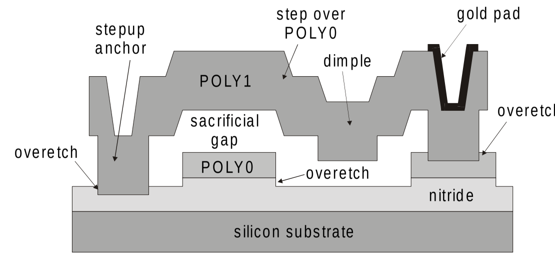

Figure 2. Profile of typical electrostatically actuated structure fabricated in MUMPs showing discontinuities, and effects of overetch. Vertical dimensions are exaggerated here and in other drawings for clarity.

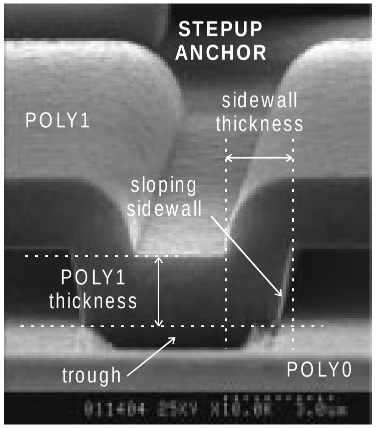

Figure 3. Scanning Electron Micrograph (SEM) of the stepup anchor of a POLY1 beam showing thickness measurement sites, and sidewall geometry. The trough in the POLY0 layer in front of the anchor is due to the patterning of the POLY1 layer after the anchor etch of the PSG.

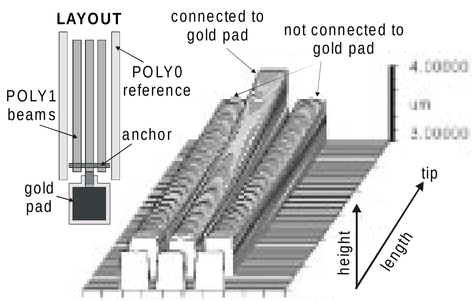

Figure 4. Interferometric image of three unloaded, freestanding POLY1 cantilevers with similar designs except that the center one is connected to a gold pad. A sketch of the layout is shown in the inset. The center cantilever curls up more. Interferometric images only show top surfaces therefore the sacrificial gap is not displayed. Heights are referenced to the POLY0 layer. These beams fabricated in

MUMPs 27 and released in a 2.5 minute HF etch are 300 µm long and anchored to the nitride layer.

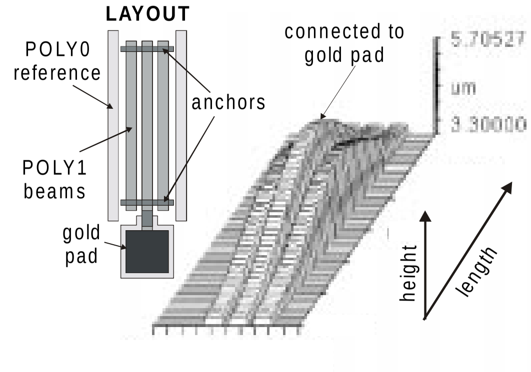

Figure 5. Interferometric image of three unloaded, freestanding POLY1 fixed-fixed beams with similar designs except that the center one is connected to a gold pad. A sketch of the layout is shown in the inset. The center beam buckles up 0.62 µm more than the other two beams indicating a higher average compressive stress. These beams fabricated in MUMPs 27 and released in a 2.5 minute HF etch are 700 µm long and anchored to the nitride layer.

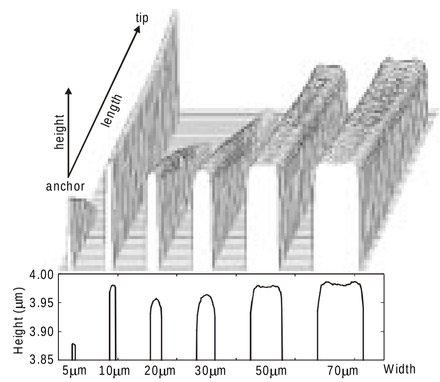

Figure 6. Interferometric image of the unloaded deflection of released cantilevers of various widths fabricated in MUMPs 25 and subjected to a 2.5 minute HF etch. The beams exhibit different degrees of curvature, and surface height variations along the direction of the width. A cross section taken near the anchors reveals more detail. Beams are anchored to nitride and have no gold connections.

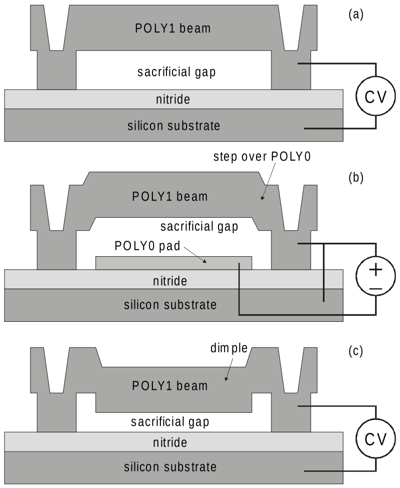

Figure 7. Profiles of electrostatically actuated beams. All beams are designed to be essentially extrusions of these 2-D profiles in order to match simulations well. (a) Beam is flat except for the anchors. Pull-in is measured by sensing the abrupt change in capacitance using an HP4275A LCR meter. (b) Beam is suspended above a POLY0 pad. Using an HP4155A Semiconductor Parameter Analyzer to source voltage and sense current, pull-in is detected when current begins to flow as the beam contacts the POLY0 pad. (c) The gap under the center portion of the beam is reduced via a dimple etch. Pull-in is sensed using the HP4275A meter as in (a).

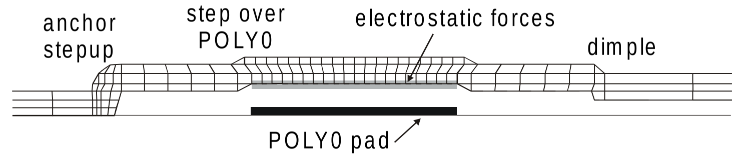

Figure 8. Mesh in Abaqus of a portion of the dual-bias-electrode structure of Fig. 14. The stepup sidewall detail and the effects of overetch are included. The solid mechanics describing beam behavior are solved using quadratic reduced-integration plane stress elements everywhere except at the anchors where plane strain elements are used. Electrostatic forces are applied to the underside of the beam as user-defined loads. For beams actuated over nitride, the forces are applied to the entire underside. For beams actuated over POLY0, the forces are applied only to the portion of the beam directly above the POLY0 as shown by the shaded region.

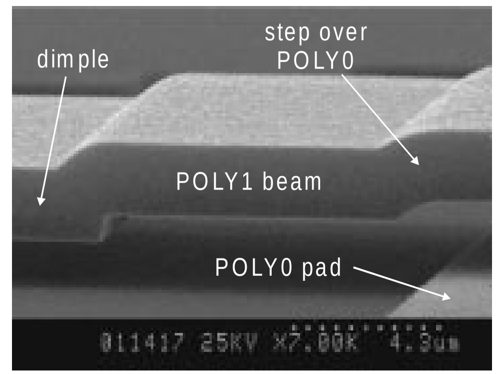

Figure 9. SEM of step over POLY0 and step into dimple. The step over POLY0 is gradual because the conformal POLY1 is itself deposited over a conformal layer of PSG. The edge of the dimple has sloping sidewalls just like the stepup anchor.

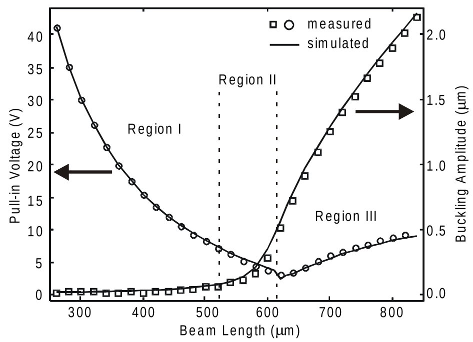

Figure 10. Pull-in voltages (left axis) and buckling amplitudes (right axis) of flat beams as functions of beam length. Three regions of pull-in behavior are demarcated. The pull-in voltage decreases with beam length until 620 μm where the pull-in voltages rise again. Significant buckling begins at that transition length. Measurements are of devices with no gold connections fabricated in MUMPs 29 and released in a 1.5 minute HF etch.

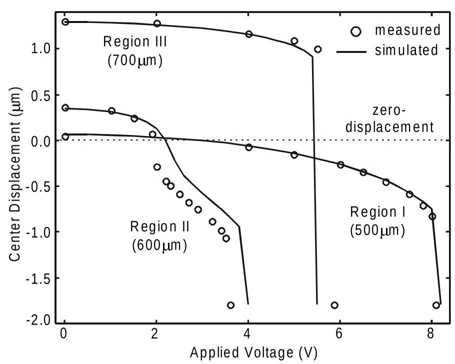

Figure 11. Three different types of pull-in behavior corresponding to the regions in Fig. 10. Beam lengths are in parentheses. The transition from Region I to Region II behavior is not very distinct.

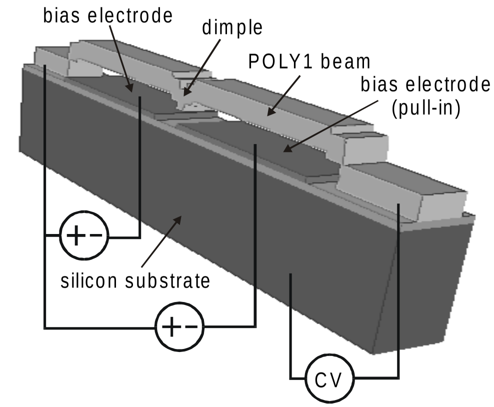

Figure 12. 3D solid model of the dual-bias-electrode structure including the effects of conformal deposition and angled sidewall etching [10]. Electrical connections are shown. Pull-in voltages at the right electrode are measured as a function of bias voltages on the left electrode. The bias voltages are applied by an HP4155A whereas pull-in is sensed using an HP4275A LCR meter. The two instruments share a common ground. The bias electrodes are close enough to the center of the beam that pull-in is still abrupt despite the leveraging action of the electrodes.

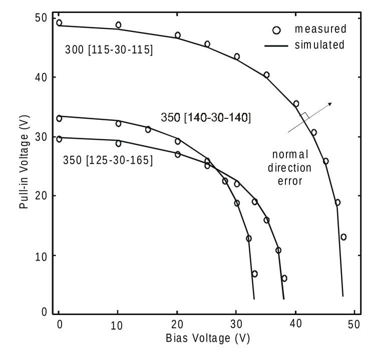

Figure 13. Pull-in voltage as a function of bias voltage for three dual-bias-electrode structures. The first number in the label is the total beam length. In the brackets

are the lengths of the pull-in electrode, the dimple, and the bias electrode. Differences between simulated and measured values determined in the direction normal to the curve are less than 2%.

Measured Thicknesses (μm)	
POLY0 (with gold)	0.52
POLY0 (without gold)	0.53
POLY1	1.97
Dimple depth	0.67
Sacrificial PSG	1.79
Nitride (electrical)	0.077
Stepup sidewall	1.80

Material Properties	
Initial biaxial stress	6.18 MPa
Young's modulus	138 GPa
Poisson's ratio	0.23

Table 1. Simulation Model Parameters